



Available online at [www.sciencedirect.com](http://www.sciencedirect.com)



International Journal of Solids and Structures 41 (2004) 6549–6571

INTERNATIONAL JOURNAL OF  
**SOLIDS and**  
**STRUCTURES**

[www.elsevier.com/locate/ijsolstr](http://www.elsevier.com/locate/ijsolstr)

# Homogenization of balanced plain weave composites with imperfect microstructure: Part I—Theoretical formulation

Jan Zeman <sup>\*</sup>, Michal Šejnoha

*Department of Structural Mechanics, Faculty of Civil Engineering, Czech Technical University in Prague,  
Thákurova 7, 166 29, Prague 6, Czech Republic*

Received 26 June 2003; received in revised form 3 May 2004  
Available online 10 June 2004

---

## Abstract

A mathematically sound computational framework is presented for the determination of a representative volume element (RVE) of plain weave fabric composites with reinforcement imperfections. Although treated as periodic two-phase composites the imperfect geometry of such material systems often precludes a straightforward representation of the RVE in terms of a simple periodic unit cell (PUC). To circumvent various limitations of simple unit cells when applied to real material systems the present contribution suggests a rigorous theoretical approach for the derivation of a reliable PUC exploiting the knowledge of the real geometry of a composite supplied by the manufacturer. It is expected that sufficient geometrical information about the real microstructure can be obtained from digitized micrographs of plain weave cross-sections that reveal the most critical imperfections caused by manufacturing processes. No attempt is therefore made to address a specific type of imperfection but rather treat them all in the combined manner. It has been demonstrated that the morphology of imperfect material systems is well-described by an appropriate set of statistical descriptors. Introducing these descriptors into a suitable optimization environment then provides a tool for the derivation of a PUC that statistically resembles the actual composite system as close as possible. In particular the parameters of the idealized unit cells follow from minimization of the objective function defined as the least square difference of the statistical descriptor related to the original microstructure and to the idealized unit cell, respectively. Once the desired geometrical parameters are determined, the finite element model of a woven composite is formulated and used to predict the overall response of the composite by the numerical homogenization method. The quality of the resulting unit cells is addressed from the point of view of effective elastic properties to examine the applicability and limitations of this procedure and to provide modeling strategy for the analysis of real-world material systems. Although applied to plain weave fabric composites the theoretical formulation presented in this paper is rather general and can be applied to any material systems with disordered or imperfect microstructures.

© 2004 Elsevier Ltd. All rights reserved.

**Keywords:** Woven composites; Periodic unit cell; Reinforcement imperfections; Microstructural statistics; Stochastic optimization; Numerical homogenization

---

<sup>\*</sup> Corresponding author. Tel.: +420-2-2435-4482; fax: +420-2-2431-0775.

E-mail address: [zemanj@cml.fsv.cvut.cz](mailto:zemanj@cml.fsv.cvut.cz) (J. Zeman).

## 1. Introduction

The remarkable material properties offered by composite materials such as high strength, light weight, corrosive resistance and affordability, etc., have resulted in their use in diverse high-performance engineering applications. Among the most prominent material systems complying with the aforementioned requirements remain polymer matrix systems reinforced either by aligned fibers, whiskers or fabrics. The popularity of latter materials, in particular, is under continuous rise due to advantageous strength/weight ratio, easiness of manipulation and low production costs.

The complex three-dimensional structure of woven fabric composites, however, makes the analysis and prediction of the overall properties of these material systems a relatively difficult task. A number of simplified analytical approaches has been proposed to obtain inexpensive closed-form estimates of the overall behavior of such material systems, starting from modified classical laminate theories approach initiated by Ishikawa and Chou (1982a,b) for simplified models of geometry and further extended by, e.g., Naik and Shembekar (1992). Alternative methods stem from the classical energy principles, see, e.g., Kregers and Malbardi (1978) and Pastore and Gowayed (1994). An application of the Mori–Tanaka method to the determination of overall elastic properties of composite was presented by Gommers et al. (1998).

In the last decade, the finite element-based methods have been employed for the analysis of woven fabric composites. In theory, the structure of woven composites can be fully described by a clearly defined periodic unit cell, which makes asymptotic homogenization techniques rather attractive for the analysis of these materials. The numerical analysis of woven composites originated from the pioneering works of Zhang and Harding (1990) for a simplified two-dimensional model and by Paumelle et al. (1990, 1991) for fully three-dimensional behavior. These studies were further followed and extended by, e.g., Dasgupta and Bhandarkar (1994), Chapman and Whitcomb (1995) and Whitcomb and Srivastava (1996). For a more detailed discussion, overview and comparison of different methods see, e.g., reviews by Cox and Flanagan (1997), Byström et al. (2000) and Chung and Tamma (1999).

Although all the above analyses rely on the idealized geometry of woven fabric composites, it is well-understood that the collective properties of these materials are to a great extent influenced by imperfections developed during the fabrication process. In this context the waviness, misalignment and/or non-uniform cross-sectional aspect ratio of tows in the longitudinal direction play the main role in assessing the overall behavior of such material systems. In this regard, the formulation of a reliable and accurate numerical model is of paramount importance. Note that simplified models of geometry, which do not account for reinforcement imperfections, are not valid even for carefully prepared laboratory samples, see Fig. 1.

On the experimental level, the effects of woven path imperfections were qualitatively investigated in several works, see, e.g., Breiling and Adams (1996), Košek and Košková (1999) and Roy (1998). The systematic classification and discussion of sources of individual types of imperfection can be found in Pastore (1993). A comprehensive quantification of the actual yarn arrangement can be also found in Košková and Vopicka (2001b), where an image analysis of composite micrographs with the help of the powerful image analyzer LUCIE was used to get the frequency spectrum of the Fourier series to describe

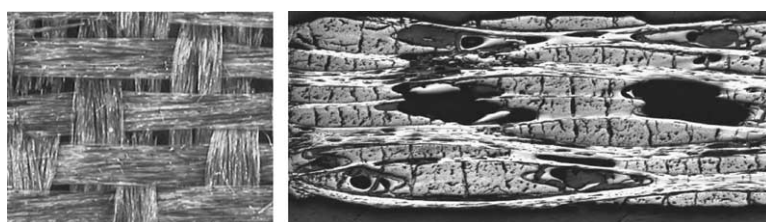


Fig. 1. An example of a textile composite micrograph. Courtesy of B. Košková, Technical University of Liberec.

the yarn shape in both woven and braided fabrics. Moreover, it has been recognized that the crimp wavefront is subject to deformation when pressed during the manufacturing process and that the frequency spectrum is therefore disordered compare to that of the uncompressed (free) fabric. Using the technique of gradual abrasion it is possible not only to retrieve the deformed shape of the yarn cross-section at various sections along the fiber tow path to a sufficient degree of accuracy but also, if needed, to assure that the cross-section goes through a center-line of the yarn over the section being analyzed. The deformation of the reinforcements can be then described by histograms of yarn angles with respect to the textile fabric plane, see Košková and Vopička (2001a) for further reference. Similar approach has been also applied in Yurgartis et al. (1993) for the determination of yarn shape and nesting in plain weave composites.

On the analytical level, these issues were incorporated into the framework of laminate theories by Shembekar and Naik (1992) who introduced a possible shift of individual layers in their model and in works of Yushanov and Bogdanovich (1998, 2000), who considered general random imperfections to the tow path and used the stiffness averaging method to obtain statistics on the overall elastic moduli. For the numerical analyses of this phenomenon see the work of Woo and Whitcomb (1997) for the three-dimensional geometry of the woven fabric composite and Byström et al. (2000) and Jekabsons and Byström (2002) for a simplified two-dimensional model where the influence of a relative shift of individual layers was carefully investigated.

In the present work, a different strategy is adopted to incorporate, at least to some extent, the reinforcement imperfections into the geometrical model of the unit cell. In particular, we follow the path set in papers by Povirk (1995) and Zeman and Šejnoha (2001). In these works, the idealized geometrical model of the analyzed composite is defined in terms of a certain periodic unit cell with geometrical parameters derived by matching microstructural statistics of a real microstructure and the searched PUC. For two-dimensional binary microstructures, the efficiency of this approach was numerically demonstrated for composites with elastic (Povirk, 1995; Zeman and Šejnoha, 2001), linearly viscoelastic (Šejnoha and Zeman, 2002), non-linearly viscoelastic (Zeman, 2003) and viscoplastic (Jia et al., 2002) phases. Moreover, using the model of plain weave geometry proposed by Kuhn and Charalambides (1999) in combination with binary images of real composites, this modeling strategy can be extended to the modeling of woven composites in a rather straightforward way.

The subject of the present work is closely related to recent papers on the problems of reconstructing random media with specified microstructural functions. In particular, Rintoul and Torquato (1997) proposed a method for the reconstruction of particulate systems based on the radial distribution function combined with the simulated annealing method. This work was further extended by Yeong and Torquato (1998a), where the isotropized lineal path and the two-point probability functions were used in the reconstruction process; the problems of a three-dimensional microstructures reconstruction from two-dimensional cross-sections (Yeong and Torquato, 1998b) and real-world materials (Mahwart et al., 2000; Talukdar et al., 2002) were also considered. The importance of using non-isotropized descriptors was recognized and addressed in Cule and Torquato (1999) and further extended by Sheehan and Torquato (2001), where the hexagonal grid sampling was advocated. Finally, the work of Rozman and Utz (2001) revealed that the non-uniqueness problems, reported in previous studies, can be attributed to artificial isotropy of optimized function and to convergence of the selected optimization method to a local minimum.

Summing up the pieces of knowledge from the modeling of composite material systems with either disordered or imperfect microstructures sets the following objectives of this introductory part of the homogenization of plain weave composites with imperfect microstructure: identify the most important types of imperfections that can be extracted from *binary images* of cross-sections of real composite systems; as a result of that define a minimum set of free geometrical parameters that should appear in the definition of the searched PUC; propose a sound mathematical approach for the determination of these parameters, and finally on the basis of well-defined artificial microstructures representing various sources of imperfections test the quality of the resulting unit cells, examine the applicability and limitations of this procedure

and provide modeling strategy for the analysis of real-world material systems. The actual modeling of real composite systems including the construction of the respective binary images as a source of input data will be the subject of the second part of this study. Nevertheless, the theoretical treatment of imperfect microstructures discussed herein is quite general and can be applied as a stand-alone procedure for the analysis of any heterogenous materials that can be supplied in the form of binary images. The application to woven composites is therefore only one specific example of the proposed methodology.

The paper is organized as follows. Section 2 briefly reviews quantification of microstructure morphology and describes the algorithms used for the analysis of the digitized microstructural images. Section 3 then introduces the geometrical model used in the current work, formulates the optimization problem to be solved and presents the used optimization algorithm. Section 4 demonstrates the application of these principles to two-layer composites with misaligned layers and addresses the quality of the unit cell from the point of view of their effective elastic properties to explore the applicability of the presented approach. The paper ends with a brief discussion of the extension and future development of the presented procedure.

In the following text,  $\mathbf{a}$ ,  $\mathbf{a}$  and  $\mathbf{A}$  denote a vector, a symmetric second-order and a fourth-order tensor, respectively. The standard summation notation is adopted, i.e., by  $\mathbf{A} : \mathbf{b}$  denotes the sum  $A_{ijkl}b_{kl}$  while  $\mathbf{a} \cdot \mathbf{b}$  stands for  $a_i b_i$ , where the summation with respect to repeated indices is used. The symbol  $\{\mathbf{a}\}$  is reserved for a column matrix or a vectorial representation of symmetric second-order tensor while the notation  $[\mathbf{L}]$  is employed for a matrix representation of a fourth-order tensor (Bittnar and Šejnoha, 1996; Bathe, 1995). Finally, for all arrays, the C programming language-style indexing is used, i.e., the first entry on an one-dimensional array  $a$  with the dimension  $N$  is denoted  $a_0$  while the last entry of the array is denoted as  $a_{N-1}$ .

## 2. Microstructure description

This section outlines evaluation of various statistical descriptors, which arise in the analysis of two-phase media with random arrangement of individual phases. With regard to the application of these principles to the analysis of two-dimensional sections of plain weave composites we focus on capturing the non-isotropy of the underling microstructure. For a more detailed discussion on quantification of microstructure morphology, see the recent monograph of Torquato (2002).

### 2.1. *n*-Point probability functions

To reflect a random character of a heterogeneous medium it is convenient to introduce a sample space  $\mathcal{S}$  defined as a collection of samples  $\alpha$  with  $p(\alpha)$  defining the probability density of  $\alpha$  in  $\mathcal{S}$ . To provide a general description of morphology of such media we consider a characteristic function of the  $r$ th phase  $\chi_r(\mathbf{x}, \alpha)$  defined as

$$\chi_r(\mathbf{x}, \alpha) = \begin{cases} 1, & \text{if } \mathbf{x} \in D_r(\alpha), \\ 0, & \text{otherwise,} \end{cases} \quad (1)$$

where  $D_r(\alpha)$  denotes the domain occupied by the  $r$ th phase. Then, the  $n$ -point probability function  $S_{r_1, \dots, r_n}$  is given by

$$S_{r_1, \dots, r_n}(\mathbf{x}_1, \dots, \mathbf{x}_n) = \int_{\mathcal{S}} \chi_{r_1}(\mathbf{x}_1, \alpha) \cdots \chi_{r_n}(\mathbf{x}_n, \alpha) p(\alpha) d\alpha. \quad (2)$$

In the following, we limit our attention to functions of the order of one and two, since higher-order functions are quite difficult to determine in practice. Therefore, description of a random medium will be restricted to information contained in the *one-point probability* function  $S_r(\mathbf{x})$  and the *two-point probability* function  $S_{rs}(\mathbf{x}_1, \mathbf{x}_2)$ , respectively.

Assuming the *statistical homogeneity* of the analyzed medium and validity of the *ergodic hypothesis*, the one and two-point probability functions reduce to (Torquato, 2002; Torquato and Stell, 1982)

$$S_r = c_r, S_{rs}(\mathbf{x}) = \frac{1}{|V|} \int_V \chi_r(\mathbf{x}, \alpha) \chi_s(\mathbf{x} + \mathbf{y}, \alpha) d\mathbf{y}, \quad (3)$$

with  $c_r$  denoting the volume fraction of the  $r$ th phase and  $|V|$  standing for the volume (area) of the analyzed sample.

Various sampling methods can be employed to determine the values of one- and two-point probability functions, starting from simple Monte–Carlo method based techniques, later refined by the sampling template approach (Smith and Torquato, 1988) to sample isotropized values of two-point probability functions. However, in order to avoid well-known problems with using isotropized values in random media reconstruction (Sheehan and Torquato, 2001; Talukdar et al., 2002; Rozman and Utz, 2001), the Fourier-transform procedure (Berryman, 1984) is employed in the present work to sample the two-point probability function. To this end, we consider a discretization of the microstructure in terms of  $W \times H$  bitmap and denote the value of characteristic function for a pixel located in the  $i$ th row and  $j$ th column as  $\chi_r(i, j)$ . Assuming the microstructure periodicity, Eq. (3) can be replaced by

$$S_r = \frac{1}{WH} \sum_{i=0}^{W-1} \sum_{j=0}^{H-1} \chi_r(i, j), \quad (4)$$

$$S_{rs}(m, n) = \frac{1}{WH} \sum_{i=0}^{W-1} \sum_{j=0}^{H-1} \chi_r(i, j) \chi_s((i + m) \% W, (j + n) \% H), \quad (5)$$

where  $a \% b$  stands for  $a$  modulo  $b$ . The sum (5) can be then replaced by the discrete Fourier transform as

$$S_{rs}(m, n) = \frac{1}{WH} \text{IDFT} \left\{ \text{DFT}\{\chi_r(m, n)\} \overline{\text{DFT}\{\chi_s(m, n)\}} \right\}, \quad (6)$$

where  $\overline{\cdot}$  denotes the complex conjugate and  $\text{DFT}\{\cdot\}$ ,  $\text{IDFT}\{\cdot\}$  stand for the discrete Fourier transform and its inverse, respectively.

Of course, the fast Fourier transform, which needs only  $\mathcal{O}(WH \log(WH) + WH)$  operations compared to the  $\mathcal{O}(W^2H^2)$  operations needed by Eq. (5), is called to carry out the numerical computation. Moreover, the possibility of using highly optimized software libraries permits to efficiently analyze even high-resolution bitmaps within a reasonable time.

## 2.2. Lineal path function

As already noted in the previous section, the determination of probability functions of the order higher than two encounters serious difficulties, both analytical and numerical. However, these functions still contain an important amount of information not correctly captured by low-order probability functions. To overcome this difficulty, one can study low-order microstructural descriptors based on a more complex fundamental function which contains more detailed information about phase connectedness and hence certain information about long-range orders. The lineal path function (Lu and Torquato, 1992), briefly discussed in this section, is a representative of such indicators.

To maintain formal similarity with the discussion on the  $n$ -point probability functions, we first introduce a random function  $\lambda_r(\mathbf{x}_1, \mathbf{x}_2, \alpha)$  as

$$\lambda_r(\mathbf{x}_1, \mathbf{x}_2, \alpha) = \begin{cases} 1, & \text{if } \mathbf{x}_1 \mathbf{x}_2 \subset D_r(\alpha), \\ 0, & \text{otherwise,} \end{cases} \quad (7)$$

i.e., a function which equals to one when the segment  $\mathbf{x}_1\mathbf{x}_2$  is contained in the  $r$ -phase for the sample  $\alpha$  and equals to zero otherwise. The lineal path function giving the probability that the  $\mathbf{x}_1\mathbf{x}_2$  segment is fully contained in the phase  $r$ , then follows directly from the ensemble averaging of this function

$$L_r(\mathbf{x}_1, \mathbf{x}_2) = \int_{\mathcal{S}} \lambda_r(\mathbf{x}_1, \mathbf{x}_2, \alpha) p(\alpha) d\alpha. \quad (8)$$

Under the assumptions of statistical homogeneity, the lineal path function simplifies, in analogy with the two-point probability function, as

$$L_r(\mathbf{x}_1, \mathbf{x}_2) = L_r(\mathbf{x}_1 - \mathbf{x}_2). \quad (9)$$

Similarly to the  $n$ -point probability function, an elementary Monte-Carlo-based simulation procedure can be used again for the evaluation of lineal path function, i.e., we randomly throw segments into a medium and count the cases when the segment is fully contained in a given phase. A computationally more intensive approach, however, can be employed following the idea of sampling template introduced in Smith and Torquato (1988).

To that end, we form a sampling template with dimensions  $T_W \times T_H$  pixels. Then, we draw  $N_d$  segments, each of them consisting of  $N_\ell(i)$  pixels, from the center of a template to the points on the template boundary separated by given discrete steps  $\Delta_W$  and  $\Delta_H$  (see Fig. 2). Sampling the values of the lineal path function for a given direction and phase starts from placing the template center at a given point found in the phase  $r$  and then marking the pixel at which the segment corresponding to the selected direction meets the other phase. Then, counters corresponding to pixels of a given segment, which are closer to the center than the marked pixel, are increased by one while the remaining ones are left unchanged. The value of the lineal path function can be then obtained either by stochastic sampling (randomly throwing template center in a medium) or deterministic sampling (the template center is successively placed in all pixels of a bitmap) and by averaging the obtained results. Moreover, the latter method allows us to actually use only a half of the sampling template, provided that the analyzed microstructure is statistically homogeneous. Note that even though this procedure basically needs only integer-based operations, it is still substantially slower than the FFT-based approach. Hence, a relatively sparse sampling template is unavoidable if one wishes to keep the efficiency of this procedure comparable to the determination of the two-point probability function.

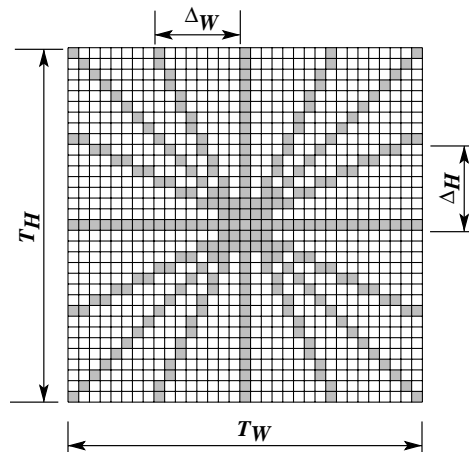


Fig. 2. An example of a sampling template.

### 3. Unit cell definition

As suggested in the introductory part, a realistic model of composite geometry is needed in order to obtain reliable estimates of both the local and overall response of real composites under certain loading conditions. However, such a model, to be statistically representative of the composite, might be quite complex leading to an enormous computational cost. The computational feasibility, on the other hand, calls for rather simple models usually specified in terms of small periodic unit cells. The present section attempts to reconcile these competing requirements by formulating a small periodic unit cell, which yet incorporates the knowledge of real composite geometry with various types of reinforcement imperfections.

#### 3.1. Geometrical model

Following the work of Košková and Vopička (2001a,b) the two-dimensional images of a tow cross-section of C/C composite laminates advocate the following set of imperfections to be addressed: deformation of the crimp waveform to account for the actual crimp height which as a result of manufacturing may considerably differ from that of free yarn, variability of the crimp height along the longitudinal path and from layer to layer and finally a mutual shift of laminate layers. Clearly, these are the most apparent irregularities in the fiber tow path that can be measured from two-dimensional data. On the contrary, this list of imperfections is almost exhausted as the only imperfection not specifically addressed in the present study is the out-of-plane yarn misalignment. To incorporate this parameter into the PUC formulation would inevitably call for three-dimensional binary images. Although techniques for constructing three-dimensional microstructural images have been recently introduced (Li et al., 1998; Nagai et al., 2001; Terada et al., 1997, and references therein), they are rather laborious and the subsequent analysis is extremely computationally demanding even for elastic materials. Moreover, it was demonstrated in Yeong and Torquato (1998b), Mahwart et al. (2000) and Roberts and Garboczi (1999) that, at least for some classes of materials, the data obtained from two-dimensional sections allow reconstructing the three-dimensional microstructural configurations with satisfactory details.

Literature offers a manifold of geometric models for the description of plain weave geometry with varying level of sophistication. In this work, the model of fabric weave composite proposed by Kuhn and Charalambides (1999) is used since it is reasonably simple to implement and directly incorporates typical features of real composites reported in Yurgartis et al. (1993). The present model is fully determined by four parameters  $a$ ,  $b$ ,  $g$  and  $h$ , see Fig. 3. For the sake of completeness, a brief discussion of the geometrical model is included in Appendix A; in this section, we restrict our attention to two-dimensional cross-sections located in the  $xz$  plane.

For the transverse cross-sectional plane located in the middle of the weave, the fill and warp bundle surface functions  $s_{\text{fill}}$  and  $s_{\text{warp}}$ , Eq. (A.8), reduce to, see Fig. 3,

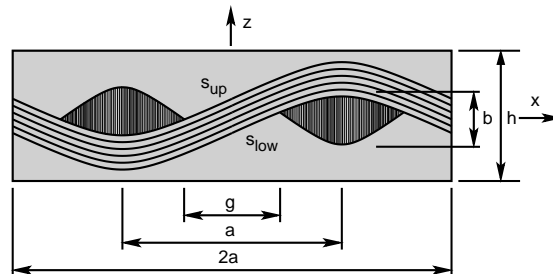


Fig. 3. Geometrical parameters of a plain weave PUC.

$$s_{\text{low}}(x) = \begin{cases} \frac{b}{2} \left( \sin\left(\frac{\pi x}{a}\right) - \frac{x(1-\delta)}{g} - \frac{1}{2}(1+\delta) \right) & 0 \leq x < \frac{g}{2} \\ -\frac{b}{2} \left( 1 + (1+\beta) \sin\left(\frac{\pi(2x-g)}{2(a-g)} - \beta\right) \right) & \frac{g}{2} \leq x \leq \frac{a}{2} \end{cases}, \quad (10)$$

$$s_{\text{up}}(x) = \begin{cases} \frac{b}{2} \left( \sin\left(\frac{\pi x}{a}\right) - \frac{x(1-\delta)}{g} + \frac{1}{2}(1+\delta) \right) & 0 \leq x < \frac{g}{2} \\ \frac{b}{2} \left( \sin\left(\frac{\pi x}{a}\right) + \delta \right) & \frac{g}{2} \leq x \leq \frac{a}{2} \end{cases}, \quad (11)$$

where coefficient  $\beta$  is defined in Eq. (A.4) and  $\delta = (1+\beta) \cos(\beta)$ . Values of function  $s_{\text{low}}$  and  $s_{\text{up}}$  for  $x > a/2$  and  $x < 0$  follow from symmetry of the PUC.

Although intended for representation of real-world composites that may generally experience an arbitrary mode of imperfections, the present idealized geometrical model of Fig. 3 builds upon a number of simplifying assumptions. In particular, it assumes balanced fabrics with constant yarn thickness and harmonic functions defining the yarn shape. In addition, as also evident from Fig. 3, the relative shift of individual layers does not appear directly as a free parameter in the present model. Finally, as a consequence of a single-layer unit cell, the model is not able to explicitly account for the nesting of individual layers as is often the case in real composite systems. One of the principle goals of the present study thus appears in identifying a class of imperfections that can be satisfactorily tackled with the proposed model and suggest possible modifications to overcome a priori introduced restrictions of the present model.

### 3.2. Objective function

Having chosen the model for the description of geometry of a PUC, one needs to define a certain objective function, which quantifies the difference between the original microstructure and the idealized periodic unit cell. Following the general procedure discussed in Section 2, the fundamental *bundle characteristic function*  $\chi_f(x, z, \alpha)$  is simply provided by the relation

$$\chi_f(x, z, \alpha) = \begin{cases} 1, & \text{if } s_{\text{low}}(x) \leq z \leq s_{\text{up}}(x) \text{ for sample } \alpha \\ 0, & \text{otherwise.} \end{cases} \quad (12)$$

This characteristic function  $\chi_f$  can be employed to discretize the PUC cross-section into the form of a  $W \times H$  bitmap. Then, assuming the periodicity of the microstructure, the two-point probability function follows from Eq. (6). Similarly, the matrix lineal path function  $L_m$  for a given digitized periodic unit cell can be determined by the sampling template method introduced in Section 2.2.

To determine “statistically” optimal parameters of the periodic unit cell, the parameters  $a, b, g$  and  $h$  are found by minimizing certain objective functions. Similarly to (Yeong and Torquato, 1998a,b; Talukdar et al., 2002), objective functions incorporating the two-point matrix probability function  $S_{mm}$ , matrix lineal path function  $L_m$  or their combination are considered,

$$F_S(\mathbf{x}) = \sum_{i=-i_{\max}}^{i_{\max}} \sum_{j=-j_{\max}}^{j_{\max}} (\bar{S}_{mm}(i, j) - S_{mm}(i, j))^2, \quad (13)$$

$$F_L(\mathbf{x}) = \sum_{i=0}^{N_d-1} \sum_{j=0}^{N_\ell(i)-1} (\bar{L}_m(i, j) - L_m(i, j))^2, \quad (14)$$

$$F_{S+L}(\mathbf{x}) = F_S(a, b, h, g) + F_L(a, b, h, g), \quad (15)$$

where  $\mathbf{x} = \{a, b, h, g\}^T$  is the vector of unknown dimensions of the PUC,  $\bar{S}_{mm}$  and  $\bar{L}_m$  are the values of  $L_m$  and  $S_{mm}$  functions corresponding to the target microstructure, parameters  $i_{\max}$  and  $j_{\max}$  define the range of points, in which  $S_{mm}$  functions are matched,  $N_d$  denotes the number of rays of a sampling template and  $N_\ell(i)$  is the number of pixels of the  $i$ th sampling ray, respectively. Then, the following optimization problem is to be solved in order to determine the optimal parameters of a periodic unit cell:

**Optimal plain weave periodic unit cell.** For a selected statistical descriptor  $D \in \{S, L, S + L\}$  find the parameters of the PUC  $\mathbf{x}$  such that

$$\mathbf{x} \in \operatorname{Argmin}_{\mathbf{x} \in \mathcal{B}} F_D(\mathbf{x}), \quad (P)$$

where  $\mathcal{B}$  denotes a set of admissible unit cell parameters,

$$\mathcal{B} = \{\mathbf{x} \in \mathbb{R}^4 : L_i \leq x_i \leq U_i, i = 1, \dots, N\}, \quad (16)$$

where  $L_i$  and  $U_i$  denote the lower and upper bounds on unit cell parameters, selected, e.g., on the basis of image analysis.

Note that the objective of the optimization problem (P) is to determine a (possibly unique) set of geometrical parameters related to a given imperfect microstructure. In particular, this implies that although morphology of the original microstructure is characterized in a statistical sense, the optimization procedure focuses on finding only optimal values and not the statistics of the individual parameters themselves.

### 3.3. Optimization algorithm

As demonstrated in Zeman (2003) and Zeman and Šejnoha (2002), the objective functions (13)–(15) are discontinuous with a large number of local plateaus. This is a direct consequence of working with bitmap images with a limited resolution. Such objective functions cannot be directly treated by classical optimization algorithms. In our previous works (Zeman and Šejnoha, 2001, 2002; Matouš et al., 2000) evolutionary algorithms showed themselves to be able to solve similar problems quite efficiently. Based on these results, the *real-encoded augmented simulated annealing* method is implemented to solve the present tasks. This method is the combination of two stochastic optimization techniques—genetic algorithm and the parallel simulated annealing (Mahfoud and Goldberg, 1995). It uses basic principles of genetic algorithms (a population of possible solutions (*individuals*), instead of one, is optimized, individuals are successively subjected to *selection* and recombination by *genetic operators* according to the value of their objective function (*fitness*)), but controls replacement of parents by the *Metropolis criterion* (see Eq. (18)). This increases the robustness of the method, since it allows a worse child to replace its parent and thus escape from local minima, which is in contradiction with the classical optimization methods. An interested reader may find further information on this subject, e.g., in Goldberg (1989) and Michalewicz (1996). The algorithmic scheme of the present implementation is briefly summarized as follows.

- (1) Randomly generate an initial population and assign fitness to each individual. Initial temperature is set to  $T_0 = T_{\max} = T\_frac{F_{\text{avg}}}$  and minimal temperature is determined as  $T_{\min} = T\_frac\_min{F_{\text{avg}}}$ , where  $F_{\text{avg}}$  is the average fitness value of the initial population.
- (2) Select an appropriate genetic operator. Each operator is assigned a certain probability of selection.
- (3) Select an appropriate number of individuals (according to the operator) and generate possible replacements. To select individuals, we apply the *normalized geometric ranking* scheme. The probability of selection of the  $i$ th individual is given by

$$p_i = q'(1 - q)^{r-1}, \quad q' = \frac{q}{1 - (1 - q)^P}, \quad (17)$$

where  $q$  is the probability of selecting the best individual in the population,  $r$  is the rank of the  $i$ th individual with respect to its fitness, and  $P$  is the population size.

(4) Apply operators to selected parent(s) to obtain possible replacement(s).

(4a) Look for an identical individual in a population. If such an individual exists, it is replaced by a new one. This operation increases the diversity of a population and thus decreases the chance of falling into a local minimum.

(4b) Replace an old individual if

$$u(0, 1) \leq \exp(F(I_{\text{old}}) - F(I_{\text{new}})) / T_t, \quad (18)$$

where  $F(\cdot)$  is the fitness of a given individual,  $T_t$  is the actual temperature and  $u(\cdot, \cdot)$  is a random number with the uniform distribution on a given interval.

(5) Steps 2–3 are performed until the number of successfully accepted individuals reaches `success_max` or selected number of steps reaches `counter_max`.

(6) Decrease temperature

$$T_{t+1} = T_{\text{mult}} \times T_t.$$

If actual temperature  $T_{t+1}$  is smaller then  $T_{\text{min}}$ , perform *reannealing*—i.e., perform step #1 for one half of the population.

(7) Steps 2–6 are repeated until the termination condition is attained.

The detailed description of this algorithm, list of used operators as well as some tests of its performance can be found in Matouš et al. (2000) and Hrstka et al. (2003). See also Zeman (2003) for values of individual parameters of this method for the current optimization problems.

#### 4. Numerical experiments

In this section, the performance and robustness of the selected global optimization method is investigated for a set of carefully chosen optimization problems. First, the ability of the algorithm to determine the parameters of a periodic unit cell with known parameters is investigated by solving the media reconstruction problem. Then, optimal unit cells are generated for artificial microstructures with predefined imperfections. Since variation of the crimp height along the fiber tow path is difficult to generate we limit our attention to two specific irregularities. Building up on the use of a single ply PUC we assume well-separated layers, an assumption not generally fulfilled in practice, and allow for the presence of layer shifts and variation of the crimp height from layer to layer only. The quality of the resulting periodic unit cell is then judged from the point of view of effective elastic properties derived from the numerical homogenization procedure.

##### 4.1. Identification problem

To test sensitivity of the optimization process with respect to the bitmap resolution, three different bitmaps with dimensions  $128 \times 16$ ,  $256 \times 32$  and  $512 \times 64$  pixels were constructed for a unit cell corresponding to parameters  $a = 10$ ,  $h = 3$ ,  $g = b = 1$ . For each bitmap the optimization algorithm was run 20 times to minimize the influence of various random circumstances. The computation was terminated if the algorithm returned a value smaller than  $10^{-6}$  or if the number of objective function evaluations exceeded 50,000. Bounds of individual parameters were set to 50% and 200% of the target values. The  $S_{\text{mm}}$ -based objective function was considered first. The matching range  $i_{\text{min}}-i_{\text{max}}$  and  $j_{\text{min}}-j_{\text{max}}$ , introduced in Eq. (13),

Table 1  
 $S_{mm}$ -based identification: number of function evaluations

Bitmap resolution	Success rate	Number of function evaluations			Total time [s]
		Min	Avg	Max	
128×16	20/20	1106	2826	6321	116
256×32	20/20	2336	3542	5320	1016
512×64	20/20	2716	4581	12,457	6648

Table 2  
Geometrical parameters of the PUC:  $S_{mm}$ -based optimization

Resolution	$a_{min}$	$a_{max}$	$h_{min}$	$h_{max}$
	$b_{min}$	$b_{max}$	$g_{min}$	$g_{max}$
128×16	9.8442	10.1010	2.9961	3.0119
256×32	9.9253	10.0217	2.9959	3.0020
512×64	9.9726	10.0259	2.9986	3.0009
128×16	0.9924	1.0065	0.9688	1.1010
256×32	0.9968	1.0002	0.9831	1.0141
512×64	0.9988	1.0009	0.9917	1.0157

was set to comply with the dimension of a unit cell. For each run, minimum and maximum values of searched geometric parameters were recorded. The results of this experiment are listed in Tables 1 and 2. In addition, Table 1 provides information on the average number of function calls and the relative time needed to complete the optimization run for individual bitmaps.<sup>1</sup> Notice that the optimization process converged for every run, which confirms the robustness of the RASA algorithm. A typical convergence progress of the optimization method, showing an average and the best individual in the population, is displayed, together with the PUC evolution, in Fig. 4a–b.

In general, see Table 1, the number of required iterations as well as the time needed for convergence increases with the bitmap resolution. Nevertheless, all considered bitmap resolutions, at least for the present problem, provide comparable results in terms of accuracy of the searched geometric characteristics.

The similar numerical experiments were repeated for the  $F_L$  and  $F_{S+L}$  objective functions for the bitmap resolution 256×32 pixels. Note that sampling templates with parameters  $T_W = T_H = H/2$  and  $\Delta_W = \Delta_H = H/8$  were used for the determination of the lineal path function  $L_{mm}$ . The statistics of the obtained numerical parameters together with the number of function calls and overall computational time are stored in Tables 3 and 4. Note that both optimization problems, being based on the  $L_m$  function, are about ten times more time consuming. Furthermore, both objective functions result in geometrical parameters determined with a precision comparable to the  $S_{mm}$ -based optimization. This suggests that the scatter of the geometrical parameters is caused solely by the discretization of the microstructure not by the objective function or the selected optimization method.

Finally, for the sake of completeness, examples of typical objective runs together with the plot of objective functions are shown in Fig. 4. To summarize this study, the presented results support the choice of the selected optimization method; furthermore, the resolution of the bitmap 256×32 is sufficient to obtain the searched geometrical parameters with a reasonable precision.

<sup>1</sup> All reported tests were performed on a computer with Intel Celeron 700 MHz processor with 256 MB RAM under the Linux operating system. The C++ code was compiled by **gcc 2.96** GNU complier with **-O3** optimization switch. The library **FFTW 2.1.3** (Ergo and Johnson, 1998) was called to compute the fast Fourier transform.

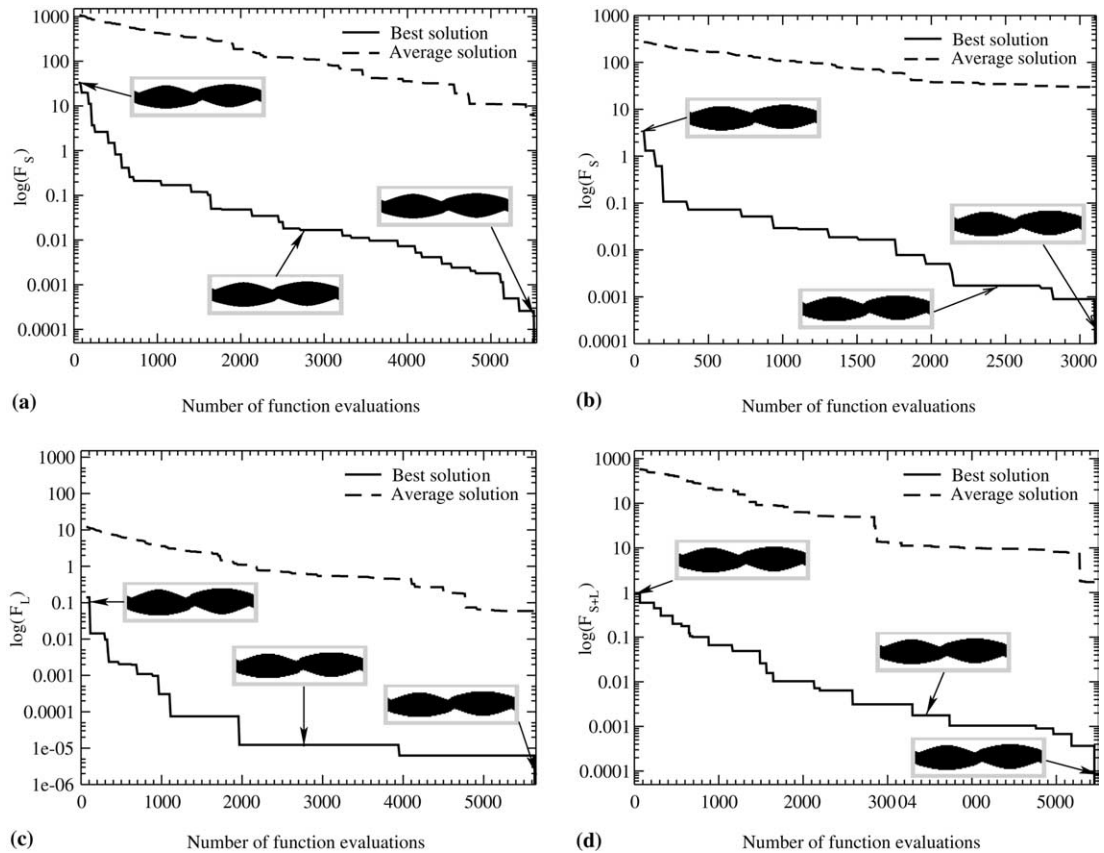


Fig. 4. Examples of typical optimization procedures, (a)  $S_{mm}$ -based objective function, bitmap resolution  $512 \times 64$  pixels, (b)  $S_{mm}$ -based objective function, bitmap resolution  $256 \times 32$  pixels, (c)  $L_m$ -based objective function, bitmap resolution  $256 \times 32$  pixels and (d)  $(S_{mm} + L_m)$ -based objective function, bitmap resolution  $256 \times 32$  pixels.

#### 4.2. Woven composites with variable crimp height and shifted layers

As a representative of digitized images of real-world multi-layered plain weave composites, a set of three artificial bitmaps exhibiting different imperfections was generated. In particular, the “samples” formed by two unit cells with different layer and bundle heights (see Fig. 5b), two identical unit cells shifted by  $a$  (see Fig. 5c) and by  $a/2$  (see Fig. 5d) are considered in this section.<sup>2</sup> Based on the results of the sensitivity analysis in the previous section, the PUC was discretized as a bitmap with the dimensions  $256 \times 92$  pixels and the PUC #2–3 were represented by bitmaps with resolution  $256 \times 64$  pixels.

For each artificial mesostructure bitmap, the statistically optimal periodic unit cell based on  $S_{mm}$ ,  $L_m$  and  $S_{mm} + L_m$  descriptors was found. The target value of the objective function for each optimization problem was set to  $10^{-6}$  and the maximum number of function evaluations was restricted to 25,000. Each optimization problem was executed ten times to verify that the global optimum was reached and to determine the

<sup>2</sup> The parameters of the bitmap 5b are  $a = 10$ ,  $h = 3$ ,  $b = g = 1$  for the lower layer and  $a = 10$ ,  $h = 4.5$ ,  $b = 1.5$ ,  $g = 1$  for the upper one; the remaining bitmaps correspond to a unit cell with  $a = 10$ ,  $h = 3$ ,  $b = g = 1$ .

Table 3

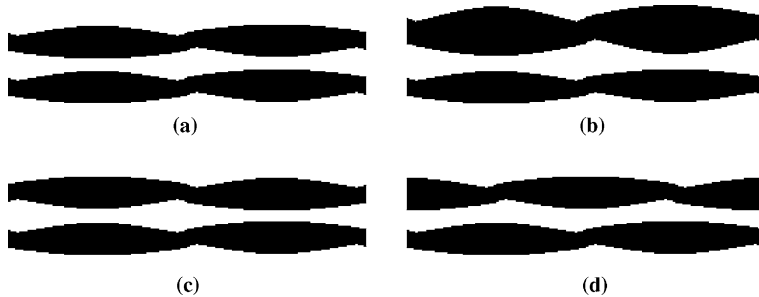
 $L_m$  and  $L_m + S_{mm}$ -based identification for  $256 \times 32$  bitmap: number of function evaluations

Descriptor	Success rate	Number of function evaluations			Total time [s]
		Min	Avg	Max	
$L_m$	20/20	3059	5842	9295	12,592
$L_m + S_{mm}$	20/20	1196	4909	30,699	11,804

Table 4

Geometrical parameters of the PUC for  $256 \times 32$  bitmap:  $L_m$ -based optimization, combined optimization

Descriptor	$a_{\min}$	$a_{\max}$	$h_{\min}$	$h_{\max}$
$L_m$	9.9227	10.0407	2.9967	3.0020
$L_m + S_{mm}$	9.9243	10.0196	2.9977	3.0023
	$b_{\min}$	$b_{\max}$	$g_{\min}$	$g_{\max}$
$L_m$	0.9973	1.0005	0.9855	1.0143
$L_m + S_{mm}$	0.9969	1.0009	0.9864	1.0139

Fig. 5. Artificial bitmaps of mesoscale geometry with typical tow misalignments, (a) ideal stacking, (b) different layer heights (PUC #1), (c) layers shifted by  $a$  (PUC #2) and (d) layers shifted by  $a/2$  (PUC #3).

scatter of geometrical parameters. The resulting optimal values obtained for individual bitmaps are stored in Table 5. As expected, the values of identified parameters differ for individual statistical descriptors. The scatter in geometrical parameters, however, is solely attributed to the problem discretization and the nature of genetic algorithms. From the material statistics point of view, recall Eqs. (13)–(15), all the unit cells are identical. See also discussion in Section 4.1. Nevertheless, the reported scatter in geometrical parameters suggests variability in the mechanical response depending on a particular unit cell being analyzed. Clearly, the actual local distribution in stress and strain fields exhibit a slight variation as a function of specific dimensions of a given unit cell. This, on the other hand, is not the case when the overall macroscopic response is examined. Moreover, since the homogenized behavior of the composite is of the main interest, the scatter of parameters in Table 5 is irrelevant in that each unit cell delivered by the optimization problem can be employed in assessing the homogenized mechanical response of the composite, see Section 4.4. To further shed a light on this subject recall that data characterizing real material systems are supplied in terms of binary images and thus entirely independent of the geometrical parameters of the idealized unit cell. In conclusion, the reliability of the optimization process is rather encouraging, particularly when judging from the precision of the identified parameters for combined objective function.

Table 5

Geometrical parameters of mesoscale PUCs

Descriptor	<i>a</i>	<i>h</i>	<i>b</i>	<i>g</i>
<i>Periodic unit cell #1</i>				
$S_{mm}$	$10.235 \pm 0.023$	$3.792 \pm 0.002$	$1.250 \pm 0.001$	$1.726 \pm 0.012$
$L_m$	$10.316 \pm 0.018$	$3.785 \pm 0.003$	$1.252 \pm 0.001$	$1.766 \pm 0.016$
$S_{mm} + L_m$	$10.098 \pm 0.015$	$3.754 \pm 0.000$	$1.249 \pm 0.000$	$1.014 \pm 0.005$
<i>Periodic unit cell #2</i>				
$S_{mm}$	$9.931 \pm 0.017$	$2.964 \pm 0.001$	$0.995 \pm 0.001$	$0.990 \pm 0.005$
$L_m$	$10.863 \pm 0.023$	$2.956 \pm 0.002$	$0.996 \pm 0.001$	$1.013 \pm 0.008$
$S_{mm} + L_m$	$9.975 \pm 0.004$	$2.964 \pm 0.001$	$0.994 \pm 0.001$	$0.988 \pm 0.005$
<i>Periodic unit cell #3</i>				
$S_{mm}$	$11.171 \pm 0.032$	$3.046 \pm 0.001$	$0.996 \pm 0.001$	$0.670 \pm 0.012$
$L_m$	$8.351 \pm 0.033$	$2.887 \pm 0.003$	$0.964 \pm 0.001$	$0.247 \pm 0.012$
$S_{mm} + L_m$	$10.841 \pm 0.016$	$3.045 \pm 0.001$	$0.998 \pm 0.001$	$0.715 \pm 0.007$

#### 4.3. Homogenization

In the next step, optimized parameters derived in previous sections are used in the geometrical model of Fig. 5 to generate an equivalent periodic unit cell that represents a real composite. Such a unit cell can be then used within the framework of the finite element method-based homogenization to arrive at the desired approximation of the effective material behavior. Although a variety of works devoted to this topic can be found in the literature, see, e.g., Paumelle et al. (1990, 1991), Byström et al. (2000), Woo and Whitcomb (2000), Michel et al. (1999), Guedes and Kikuchi (1991) and Kouznetsova et al. (2001), the homogenization procedure for the “stress-control” problem, in the terminology of Michel et al. (1999), is briefly reviewed here for the sake of completeness.

##### 4.3.1. Problem formulation

To introduce the subject, consider a plain weave composite PUC with the local coordinate systems defined such that the local  $x_1^\ell$  axis is aligned with the fiber tow direction. Further suppose that the PUC is subjected to a prescribed overall stress  $\Sigma$ . Due to assumed periodicity of the microstructure, the local displacement field  $\mathbf{u}(\mathbf{x})$  on mesoscale admits the following decomposition

$$\mathbf{u}(\mathbf{x}) = \mathbf{E} \cdot \mathbf{x} + \mathbf{u}^*(\mathbf{x}), \quad (19)$$

where  $\mathbf{u}^*(\mathbf{x})$  represents a periodic fluctuation of the local displacement field due to the presence of heterogeneities and  $\mathbf{E}$  is the overall strain tensor. The local strain tensor then assumes the form

$$\varepsilon(\mathbf{x}) = \mathbf{E} + \varepsilon^*(\mathbf{x}), \quad (20)$$

where the fluctuating part  $\varepsilon^*(\mathbf{x})$  vanishes under volume averaging. The goal now becomes the evaluation of local fields within the mesoscopic unit cell and then their averaging to receive the searched macroscopic response. In doing so, we first write the principle of virtual work (the Hill–Mandel lemma) in the form

$$\delta\mathbf{E} : \Sigma = \langle \delta\varepsilon(\mathbf{x}) : \sigma(\mathbf{x}) \rangle = \langle \delta\varepsilon^\ell(\mathbf{x}) : \sigma^\ell(\mathbf{x}) \rangle = \langle (\delta\mathbf{E}^\ell + \delta\varepsilon^\ell(\mathbf{x})) : \sigma^\ell(\mathbf{x}) \rangle, \quad (21)$$

where  $\langle \cdot \rangle$  now stands for averaging with respect to the PUC and  $\cdot^\ell$  is used to denote a quantity in a local coordinate system. The stress field written in the local coordinate system then reads

$$\sigma^\ell(\mathbf{x}) = \mathbf{L}^\ell(\mathbf{x}) : (\mathbf{E}^\ell + \varepsilon^{*\ell}(\mathbf{x})), \quad (22)$$

with  $\sigma^\ell(\mathbf{x})$  representing the local stress field,  $\mathbf{L}^\ell$  is the material stiffness tensor. Relating the strain tensors in the local and global coordinate systems by well-known relations  $\mathbf{E}^\ell = \mathbf{T}_\varepsilon : \mathbf{E}$ ,  $\varepsilon^{*\ell} = \mathbf{T}_\varepsilon : \varepsilon^*$ , see, e.g., (Bittnar and Šejnoha, 1996), and inserting Eq. (22) into Eq. (21) yields the stationarity conditions of a given problem in the form

$$\delta\mathbf{E} : \Sigma = \delta\mathbf{E} : \langle \mathbf{T}_\varepsilon(\mathbf{x}) : [\mathbf{L}^\ell(\mathbf{x}) : \mathbf{T}_\varepsilon(\mathbf{x}) : (\mathbf{E} + \varepsilon^*(\mathbf{x}))] \rangle, \quad (23)$$

$$0 = \langle \delta\varepsilon^*(\mathbf{x}) : \mathbf{T}_\varepsilon(\mathbf{x}) : [\mathbf{L}^\ell(\mathbf{x}) : \mathbf{T}_\varepsilon(\mathbf{x}) : (\mathbf{E} + \varepsilon^*(\mathbf{x}))] \rangle, \quad (24)$$

that has to be satisfied for all kinematically admissible variations  $\delta\mathbf{E}$  and  $\delta\varepsilon^*$ .

#### 4.3.2. Discretization

To obtain an approximate solution of the above system of equations, the standard conforming finite element method discretization is employed. We start from decomposing the mesoscale periodic unit cell  $Y$  into  $N_e$  disjoint elements  $Y_e$  with the discretization respecting the interfaces between individual tows and the matrix phase. Employing the engineering notation (Bittnar and Šejnoha, 1996; Bathe, 1995), the approximation of the fluctuating part of the displacement field  $\mathbf{u}^*$ , written in the *global* coordinate system, yields

$$\{\mathbf{u}^*(\mathbf{x})\} = [\mathbf{N}(\mathbf{x})]\{\mathbf{r}\}, \quad (25)$$

where  $[\mathbf{N}]$  represents, as usual, the matrix of shape functions for a given partition of the unit cell and  $\{\mathbf{r}\}$  is the vector of unknown degrees of freedom. The corresponding approximation of the strain field is then provided by

$$\{\varepsilon(\mathbf{x})\} = \{\mathbf{E}\} + [\mathbf{B}(\mathbf{x})]\{\mathbf{r}\}, \quad (26)$$

where  $[\mathbf{B}]$  is the strain–displacement matrix. Introducing Eq. (26) into Eq. (21) gives, for any kinematically admissible strains  $\{\delta\varepsilon^*\} = [\mathbf{B}]\{\delta\mathbf{r}\}$  and  $\{\delta\mathbf{E}\}$ , the associated system of linear equations in the form

$$\begin{bmatrix} \mathbf{K}_{11} & \mathbf{K}_{12} \\ \mathbf{K}_{12}^T & \mathbf{K}_{22} \end{bmatrix} \begin{Bmatrix} \mathbf{E} \\ \mathbf{r} \end{Bmatrix} = \begin{Bmatrix} \Sigma \\ 0 \end{Bmatrix}. \quad (27)$$

The individual stiffness matrices and vectors of generalized nodal forces are obtained by the assembly of contributions from individual elements,

$$\begin{aligned} [\mathbf{K}_{11}] &= \sum_{e=1}^{N_e} [\mathbf{K}_{11,e}], \quad \text{where } [\mathbf{K}_{11,e}] = \frac{1}{|Y_e|} \int_{Y_e} [\mathbf{T}_{\varepsilon,e}]^T [\mathbf{L}_{\text{meso},e}] dY_e, \\ [\mathbf{K}_{12}] &= \sum_{e=1}^{N_e} [\mathbf{K}_{12,e}], \quad \text{where } [\mathbf{K}_{12,e}] = \frac{1}{|Y_e|} \int_{Y_e} [\mathbf{T}_{\varepsilon,e}]^T [\mathbf{L}_{\text{meso},e}] [\widehat{\mathbf{B}}_e] dY_e, \\ [\mathbf{K}_{22}] &= \sum_{e=1}^{N_e} [\mathbf{K}_{22,e}], \quad \text{where } [\mathbf{K}_{22,e}] = \frac{1}{|Y_e|} \int_{Y_e} [\widehat{\mathbf{B}}_e]^T [\mathbf{L}_{\text{meso},e}] [\widehat{\mathbf{B}}_e] dY_e, \end{aligned} \quad (28)$$

where the “rotated” displacement-strain matrix  $[\widehat{\mathbf{B}}_e]$  is defined by the relation  $[\widehat{\mathbf{B}}_e] = [\mathbf{T}_{\varepsilon,e}] [\mathbf{B}_e]$  and  $\mathbf{A}$  stands for the assembly operation (Bathe, 1995). The local-global transformation can be, e.g., easily parametrized by the Euler angles determined from relations (A.10) and (A.11). Note that in the present implementation, linear tetrahedral elements are used and the values of Euler angles are related to the center of gravity of each element and are supposed to remain constant on a given element. Furthermore, the periodicity condition for the fluctuating field  $\mathbf{u}^*$  is accounted for through multi-point constraints, see (Michel et al., 1999).

Finally, eliminating the fluctuating displacements from the system (27) allows us to write the homogenized constitutive law in the form

$$\{\Sigma\} = [\mathbf{L}^{\text{fem}}]\{\mathbf{E}\}, \quad \text{where } [\mathbf{L}^{\text{fem}}] = [\mathbf{K}_{11}] - [\mathbf{K}_{12}][\mathbf{K}_{22}]^{-1}[\mathbf{K}_{12}]^T. \quad (29)$$

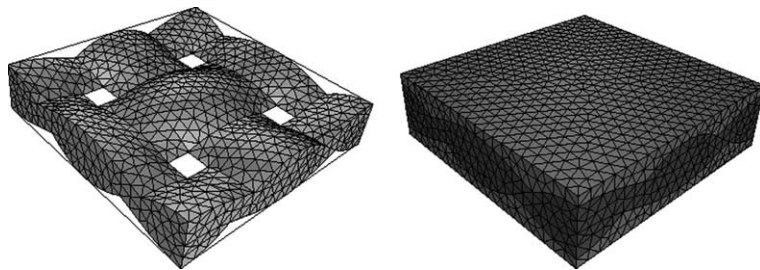


Fig. 6. Plain weave finite element meshes.

An important step of the mesoscale modeling is preparation of a 3D mesh of warp and fill bundles and matrix phase complying with the requirements of mesh periodicity. In the current work, the principles of matched mesh generation (Wentorf et al., 1999) were implemented into Advancing Front method-based automated mesh generator **T3D** (Rypl, 1998). Examples of tetrahedral meshes of a plain weave unit cell generated by this algorithm are displayed in Figs. 6 and 7.

#### 4.4. Results

As the first step, the effect of scatter of identified parameters is addressed. The material properties of matrix and bundle were taken from (Zeman and Šejnoha, 2001), and are listed in Table 6.

The minimum and maximum dimensions were taken from the  $S_{mm}$ -based identification problem for the bitmap dimensions  $256 \times 32$ , see Table 2. The results stored in Table 7 show that the difference in effective elastic moduli due to uncertainty in mesoscale PUC parameters is approximately comparable to the differences found by uniform mesh refinement (Zeman, 2003). Moreover, the deviation of the  $L_{11}^{\text{fem}}$  entry can be attributed to a relatively large difference in the bundle volume fraction  $c_f$  for the analyzed unit cells. These results thus further promote selection of an arbitrary unit cell resulting from the optimization problem as a suitable one when estimating the macroscopic response of woven composites. See also discussion in Section 4.2.

Finally, we present the comparison of effective elastic properties for the target bitmaps and corresponding statistically optimized unit cells obtained in Section 4.2. The finite element meshes corresponding to the target mesostructure appear in Fig. 7,<sup>3</sup> while the effective elastic properties of the target microstructure and the statistically optimized unit cells are stored in Table 8.

Evidently, the best correspondence between the artificial micrographs and the periodic unit cell was reached for the PUC microstructure where the optimization procedure predicts the in-plane properties with approximately the same variation as the one resulting from uniform mesh size refinement (Zeman, 2003). Note that analogously to problems of random media reconstruction, the combined optimization procedure yields the best results. The periodic unit cell based on parameters identified for PUC #2 correctly predicts the bundle volume fraction; it does not, however, take into account the different inclination of tows in individual layers which results in a slight overestimation of  $L_{11}^{\text{fem}}$  modulus. The most severe differences can be observed for the PUC #3 microstructure. As follows from Table 5, all the optimized unit cell exhibit substantially smaller value of gap between individual tows  $g$  to accommodate the layer shift present in the target micrograph, which leads to overestimating the bundle volume fraction resulting in a higher value of the in-plane component  $L_{11}^{\text{fem}}$ .

<sup>3</sup> Note that in the mesh generation procedure, the unit cells were shifted by  $a/2$  compared to bitmaps displayed in Fig. 5.

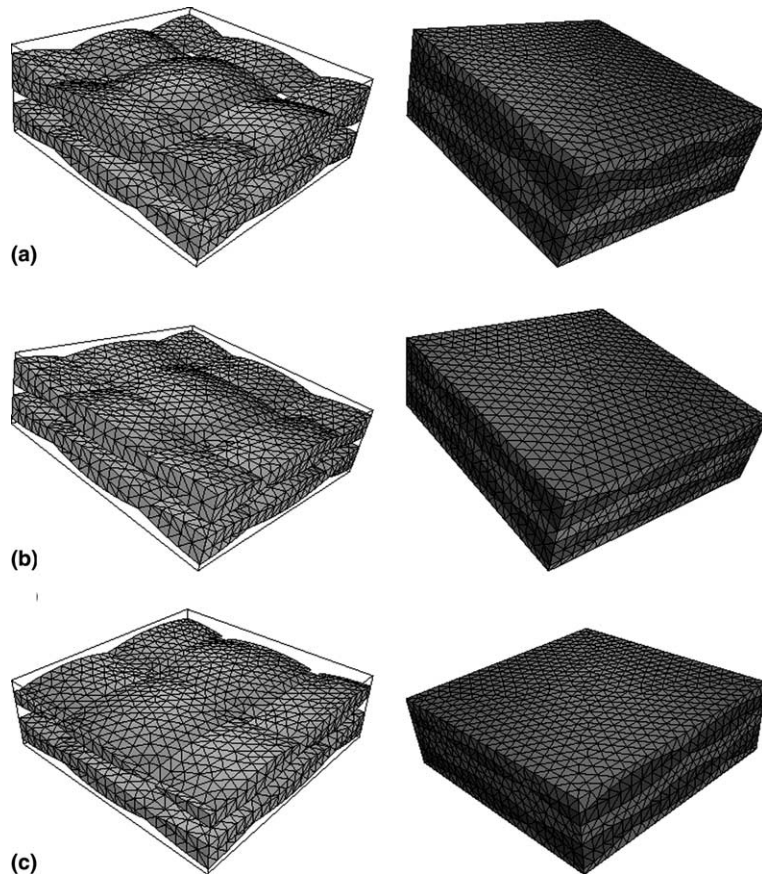


Fig. 7. Mesoscale meshes, (a) PUC, (b) PUC #2 and (c) PUC #3.

Table 6  
Elastic material properties

Bundle properties [GPa]								
$L_{11}^\ell$	$L_{22}^\ell$	$L_{33}^\ell$	$L_{12}^\ell$	$L_{13}^\ell$	$L_{23}^\ell$	$L_{44}^\ell$	$L_{55}^\ell$	$L_{66}^\ell$
176.8	10.74	10.72	6.897	6.897	6.319	2.216	4.861	4.861
Matrix properties [GPa]								
$E_A$	$E_T$	$G_T$	$\nu_A$					
5.5	5.5	1.96	0.40					

Table 7  
Effects of uncertainties in mesoscale PUC dimensions

Dimensions	$L_{11}^{\text{fem}}$ [GPa]	$L_{12}^{\text{fem}}$ [GPa]	$L_{33}^{\text{fem}}$ [GPa]	$L_{44}^{\text{fem}}$ [GPa]	$L_{66}^{\text{fem}}$ [GPa]	$c_f$
Minimal	25.247	7.496	11.371	2.264	2.965	0.3674
Target	25.250	7.494	11.370	2.265	2.966	0.3678
Maximal	25.217	7.508	11.384	2.247	2.922	0.3554

Table 8

Effective properties of statistically optimized mesoscale PUCs

Descriptor	$L_{11}^{\text{fem}}$ [GPa]	$L_{12}^{\text{fem}}$ [GPa]	$L_{33}^{\text{fem}}$ [GPa]	$L_{44}^{\text{fem}}$ [GPa]	$L_{66}^{\text{fem}}$ [GPa]	$c_f$
<i>Periodic unit cell #1</i>						
$S_{\text{mm}}$	21.100	7.499	11.401	2.265	2.868	0.3386
$L_{\text{m}}$	22.698	7.503	11.410	2.235	2.842	0.3312
$S_{\text{mm}} + L_{\text{m}}$	23.334	7.490	11.383	2.255	2.925	0.3567
Target	23.324	7.453	11.384	2.269	2.963	0.3678
<i>Periodic unit cell #2</i>						
$S_{\text{mm}}$	25.341	7.500	11.375	2.257	2.947	0.3635
$L_{\text{m}}$	26.309	7.494	11.372	2.259	2.959	0.3671
$S_{\text{mm}} + L_{\text{m}}$	25.121	7.495	11.376	2.256	2.956	0.3629
Target	24.786	7.467	11.370	2.266	2.965	0.3678
<i>Periodic unit cell #3</i>						
$S_{\text{mm}}$	27.629	7.471	11.362	2.268	2.997	0.3752
$L_{\text{m}}$	27.464	7.393	11.349	2.279	3.027	0.3872
$S_{\text{mm}} + L_{\text{m}}$	27.095	7.473	11.371	2.258	2.966	0.3678
Target	24.694	7.416	11.374	2.273	2.972	0.3670

## 5. Conclusions

In the first part of the present work, a simple and intuitive approach to the determination of idealized periodic unit cells based on microstructural statistics has been proposed. In particular, the reconstruction based on the two-point probability function, the lineal path function and their combination has been considered. The applicability and limitations of the present procedure have been demonstrated by analyzing artificial binary images of two-layer composite materials with relative shift of individual layers. The geometrical parameters of the periodic unit cells, following from the optimization analysis, have been employed to formulate the finite element model and to determine the effective elastic properties of the resulting composite.

The obtained results allow us to conclude that the proposed procedure can be efficiently used for multi-layered composites with possibly varying layers heights provided that the relative shift of individual layers is not very large or approximately equal to the unit cell half-width. In the opposite case, however, it appears to be necessary to formulate the optimized unit cell in terms of at least two-layered composite. Although increasing the modeling complexity such a modification directly allows for possible yarn contact in the geometrical model. This step thus overcomes the main obstacle of having well-separated layers of laminate, an assumption attributed to the use of a single ply PUC. In addition, the present study also revealed another geometrical aspect of real plain weave composites linked to the differences in cross-sections corresponding to planes  $x = \pm a$  and  $y = \pm a$ , see Fig. 7c. Clearly, to properly account for that calls for microstructural information supplied in the form of bitmaps taken from several locations of a composite in two orthogonal directions rather than for only one bitmap considered in this work. This generalization, together with the examples of real-world microstructures, will be considered in the forthcoming second part of this paper (Tomková et al., in preparation).

In summary, the present theoretical part clearly confirmed the applicability of the proposed approach in modeling of real material systems with possible imperfections in terms of a statistically equivalent PUC. Combining material statistics up to second-order statistical moments with a genetic algorithm based optimizer provides a powerful tool in the search for such a unit cell, which though computationally more simple but less expensive when compared to an equivalent sample of a real composite is able to incorporate most important geometrical items of actual materials. It can be expected that statistically similar PUCs will

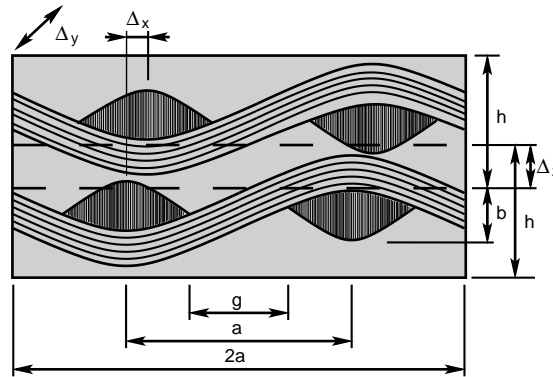


Fig. 8. Two-ply periodic unit cell.

geometrically resemble the real material systems thus provide an identical mechanical response when subjected to the same boundary and loading conditions. As also suggested by the present study the complexity of the assumed PUC directly depends on the complexity of the material system being analyzed. In particular, referring to the plain weave composites the originally proposed single ply PUC seems to be too simple to satisfactorily address even the basic set of geometrical imperfections typical for the laminate. Thus the most critical outcome of this contribution is a new two-layer PUC evident from Fig. 8 that accounts for most of the geometrical imperfections that can be measured from *binary images* of real material systems, recall Fig. 1.

In comparison with a single ply PUC, Fig. 3, the new PUC introduces three additional geometrical parameters  $\Delta_x$ ,  $\Delta_y$  and  $\Delta_z$  that describe the relative shift of individual layers in a corresponding direction. Using these parameters then opens a way to capturing, at least to some extent, the nesting of individual layers in real composites caused by the manufacturing process reported in Yurgartis et al. (1993), see also Fig. 1.

## Acknowledgements

We would like to express our thanks to Dr. Daniel Rypl for numerous discussions and support while solving problems of mesh generation. The financial support of this work provided by CAĞR grants no. 106/03/0180, no. 103/01/D052 and partially also by the research project MSM 210000003 is gratefully acknowledged.

## Appendix A. Woven composite geometrical model

The profile of the warp tow centroid  $p_c$  is described by the relation (Fig. 9)

$$p_c(x) = -\sin\left(\frac{\pi x}{a}\right), \quad (A.1)$$

while the profile of the fill tow centroid follows from the previous relation by an appropriate change of  $x$  and  $y$  coordinates and the sign (see Eq. (A.8)).

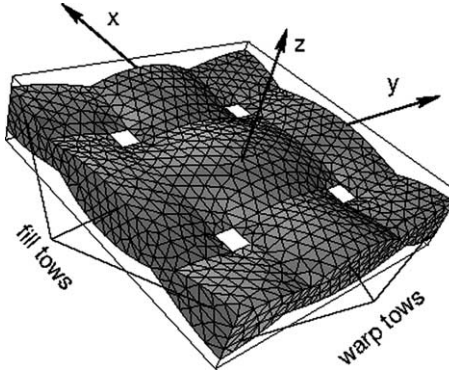


Fig. 9. Schematic representation plain weave geometry.

To maintain compatibility between warp and fill tows, the internal profiles of tows  $p_i$  are provided by

$$p_i(x) = \sin\left(\frac{\pi|x|}{a}\right). \quad (\text{A.2})$$

The external profile  $p_e$  is derived from analogous relation with amplitude modified to take into account a non-symmetry of tows and the presence of the gap between tows  $g$ ,

$$p_e(x) = (1 + \beta) \sin\left(\frac{\pi(|x| - g/2)}{a - g}\right) - \beta, \quad (\text{A.3})$$

with the coefficient  $\beta$  defined as

$$\beta = \sin\left(\frac{\pi g}{2a}\right). \quad (\text{A.4})$$

The auxiliary functions  $R$ ,  $F_H$  and  $F_R$  are used to linearly interpolate these one-dimensional functions in order to obtain representation of lower and upper surfaces of individual tows,

$$F_H(x) = H\left(|x| - \frac{g}{2}\right) - H\left(|x| + \frac{g}{2} - a\right), \quad (\text{A.5})$$

$$R(x) = \begin{cases} x/g + 1/2, & |x| \leq g/2, \\ H(x), & g/2 < |x| \leq a - g/2, \\ (\text{sgn}(x)a - x)/g + 1/2, & a - g/2 < |x| \leq a, \end{cases} \quad (\text{A.6})$$

$$F_R(\eta, x, y) = R(\eta \text{sgn}(y)x), \quad (\text{A.7})$$

where  $H$  stands for the Heaviside function,  $\text{sgn}$  denotes the signum function and parameter  $\eta = 1$  is used for the upper surface of a tow while  $\eta = -1$  corresponds to the lower surface of a tow. Finally, the warp and fill tow surfaces are determined by

$$s_{\text{warp}}(\eta, x, y) = s_{\text{tow}}(\eta, x, y), s_{\text{fill}}(\eta, x, y) = -s_{\text{tow}}(-\eta, y, x), \quad (\text{A.8})$$

where the general tow surface function  $s_{\text{tow}}(\eta, x, y)$  for positions  $|x| \leq a$  and  $|y| \leq a$  is defined as

$$s_{\text{tow}}(\eta, x, y) = \frac{b}{2} F_H(y) (\text{sgn}(y)p_e(x) + \eta F_R(\eta, x, y)p_i(y) + \eta F_R(-\eta, x, y)p_e(y)). \quad (\text{A.9})$$

Finally, the orientation of fibers within the tows is assumed to be parallel to the centroid axes of the tows; the corresponding angles of rotation are given by

$$\theta_y^{\text{warp}}(x, y) = \arctan \left( -\frac{\pi b}{2a} \text{sgn}(y) \cos\left(\frac{\pi x}{a}\right) \right), \quad (\text{A.10})$$

$$\theta_x^{\text{fill}}(x, y) = \arctan \left( -\frac{\pi b}{2a} \text{sgn}(x) \cos\left(\frac{\pi y}{a}\right) \right). \quad (\text{A.11})$$

## References

Bathe, K.J., 1995. Finite Element Procedures, second ed. Prentice Hall.

Berryman, J.G., 1984. Measurement of spatial correlation functions using image processing techniques. *Journal of Applied Physics* 57 (7), 2374–2384.

Bittnar, Z., Šejnoha, J., 1996. Numerical Methods in Structural Engineering. ASCE Press.

Breiling, K., Adams, D., 1996. Effects of layer nesting on compression-loaded 2-D woven textile composites. *Journal of Composite Materials* 30 (15), 1710–1728.

Byström, J., Jekabsons, N., Varna, J., 2000. An evaluation of different models for prediction of elastic properties of woven composites. *Composites Part B: Engineering* 31 (1), 7–20.

Chapman, C., Whitcomb, J., 1995. Effect of assumed tow architecture on predicted moduli and stresses in plain weave composites. *Journal of Composite Materials* 29 (16), 2134–2159.

Chung, P.W., Tam, K.K., 1999. Woven fabric composites—developments in engineering bounds, homogenization and applications. *International Journal for Numerical Methods in Engineering* 45 (12), 1757–1790.

Cox, B., Flanagan, G., 1997. Handbook of analytical methods for textile composites. NASA Contractor Report 4750, Langley Research Center. Available from <<http://techreports.larc.nasa.gov/ltrs>>.

Cule, D., Torquato, S., 1999. Generating random media from limited microstructural information via stochastic optimization. *Journal of Applied Physics* 86 (6), 3428–3437.

Dasgupta, A., Bhandarkar, S., 1994. Effective thermomechanical behavior of plain-weave fabric-reinforced composites using homogenization theory. *Journal of Engineering Materials and Technology—Transactions of the ASME* 116 (1), 99–105.

Erigo, M., Johnson, S., 1998. FFTW: an adaptive software architecture for the FFT. In: Proceedings of the 1998 IEEE International Conference on Acoustics, Speech and Signal Processing, ICASSP98, vol. 3. IEEE, New York, pp. 1381–1384. Available from <<http://www.fftw.org>>.

Goldberg, D., 1989. Genetic Algorithms in Search, Optimization and Machine Learning. Addison-Wesley.

Gommers, B., Verpoest, I., Van Houtte, P., 1998. The Mori–Tanaka method applied to textile composite materials. *Acta Materialia* 46 (6), 2223–2235.

Guedes, J., Kikuchi, N., 1991. Preprocessing and postprocessing for materials based on the homogenization method with adaptive finite elements method. *Computer Methods in Applied Mechanics and Engineering* 83 (2), 143–198.

Hrstka, O., Kučerová, A., Leps, M., Zeman, J., 2003. A competitive comparison of different types of evolutionary algorithms. *Computers & Structures* 81 (18–19), 1979–1990.

Ishikawa, T., Chou, T., 1982a. Elastic behavior of woven hybrid composites. *Journal of Composite Materials* 16, 2–19.

Ishikawa, T., Chou, T., 1982b. Stiffness and strength behavior of woven fabric composites. *Journal of Materials Science* 17 (11), 3211–3220.

Jekabsons, N., Byström, J., 2002. On the effect of stacked fabric layers on the stiffness of a woven composite. *Composites Part B: Engineering* 33 (8), 619–629.

Jia, S., Raiser, G., Povirk, G., 2002. Modeling the effects of hole distribution in perforated aluminum sheets i: representative unit cells. *International Journal of Solids and Structures* 39 (9), 2517–2532.

Košek, M., Košková, B., 1999. Analysis of yarn wavy path periodicity of textile composites using discrete Fourier transform. In: Proceeding of International Conference on Composite Engineering ICCE/6. Orlando, Florida, pp. 427–429.

Košková, B., Vopička, S., 2001a. Determination of yarn waviness parameters for C/C woven composites. In: Proceedings of International Conference CARBON'01. Lexington (KY, USA), pp. 1–6.

Košková, B., Vopička, S., 2001b. Geometrical aspects of woven composite structure. In: Proceedings of International Conference “Reinforced Plastics”. Karlovy Vary, Czech Republic, pp. 96–102.

Kouznetsova, V., Brekelmans, W.A.M., Baaijens, P.T., 2001. An approach to micro–macro modeling of heterogeneous materials. *Computational Mechanics* 27 (1), 37–48.

Kregers, A., Malbardis, Y., 1978. Determination of the deformability of three-dimensionally reinforced composites by stiffness averaging method. *Polymer Mechanics* 1 (1), 3–8.

Kuhn, J.L., Charalambides, P.G., 1999. Modeling of plain weave fabric composite geometry. *Journal of Composite Materials* 33 (3), 188–220.

Li, M., Ghosh, S., Rouns, T.N., Weiland, H., Richmond, O., Hunt, W., 1998. Serial sectioning method in the construction of 3-D microstructures for particle-reinforced MMCs. *Materials Characterization* 41 (2–3), 81–95.

Lu, B., Torquato, S., 1992. Lineal-path function for random heterogeneous materials. *Physical Review E* 45 (2), 922–929.

Mahfoud, S., Goldberg, D., 1995. Parallel recombinative simulated annealing: a genetic algorithm. *Parallel Computing* 21 (1), 1–28.

Mahwart, C., Torquato, S., Hilfer, R., 2000. Stochastic reconstruction of sandstones. *Physical Review E* 62 (1), 893–899.

Matouš, K., Leps, M., Zeman, J., Šejnoha, M., 2000. Applying genetic algorithms to selected topics commonly encountered in engineering practice. *Computer Methods in Applied Mechanics and Engineering* 190 (13–14), 1629–1650.

Michalewicz, Z., 1996. *Genetic Algorithms + Data Structures = Evolution Programs*, third ed. Springer-Verlag.

Michel, J.C., Moulinec, H., Suquet, P., 1999. Effective properties of composite materials with periodic microstructure: a computational approach. *Computer Methods in Applied Mechanics and Engineering* 172, 109–143.

Nagai, G., Yamada, T., Wada, A., 2001. Accurate modeling and fast solver for the stress analysis of concrete materials based on digital image processing technique. *International Journal for Computational Civil and Structural Engineering* 1.

Naik, N., Shembekar, P., 1992. Elastic behavior of woven fabric composites. 1. Lamina analysis. *Journal of Composite Materials* 26 (15), 2196–2225.

Pastore, C., 1993. Quantification of processing artifacts in textile composites. *Composites Manufacturing* 4 (4), 217–226.

Pastore, C., Gowayed, Y., 1994. A self-consistent fabric geometry model—modification and application of a fabric geometry model to predict the elastic properties of textile composites. *Journal of Composites Technology & Research* 16 (1), 32–36.

Paumelle, P., Hassim, A., Léné, F., 1990. Composites with woven reinforcements: calculation and parameter analysis of the properties of the homogeneous equivalent. *Recherche Aerospatiale* 1, 1–12.

Paumelle, P., Hassim, A., Léné, F., 1991. Microstress analysis in woven composite structure. *Recherche Aerospatiale* 6, 47–62.

Povirk, G.L., 1995. Incorporation of microstructural information into models of two-phase materials. *Acta Metallurgica et Materialia* 43 (8), 3199–3206.

Rintoul, M., Torquato, S., 1997. Reconstruction of the structure of dispersions. *Journal of Colloid and Interface Science* 186 (2), 467–476.

Roberts, A., Garboczi, E., 1999. Elastic properties of a tungsten–silver composite by reconstruction and computation. *Journal of the Mechanics and Physics of Solids* 47 (10), 2029–2055.

Roy, A.K., 1998. Comparison of in situ damage assessment in unbalanced fabric composite and model laminate of planar (one-directional) crimping. *Composites Science and Technology* 58 (11), 1793–1801.

Rozman, M.G., Utz, M., 2001. Efficient reconstruction of multiphase morphologies from corellation functions. *Physical Review E* 63, 066701-1–066701-8.

Rypl, D., 1998. Sequential and parallel generation of unstructured 3D meshes. Vol. 2 of CTU Reports. Czech Technical University in Prague.

Šejnoha, M., Zeman, J., 2002. Overall viscoelastic response of random fibrous composites with statistically quasi uniform distribution of reinforcements. *Computer Methods in Applied Mechanics and Engineering* 191 (44), 5027–5044.

Sheehan, N., Torquato, S., 2001. Generating microstructures with specified correlation functions. *Journal of Applied Physics* 89 (1), 53–60.

Shembekar, P., Naik, N., 1992. Elastic behavior of woven fabric composites. 2. Laminate analysis. *Journal of Composite Materials* 26 (15), 2226–2246.

Smith, P., Torquato, S., 1988. Computer simulation results for the two-point probability function of composite media. *Journal of Computational Physics* 76, 176–191.

Talukdar, M., Torsaeter, O., Ionnidis, M., 2002. Stochastic reconstruction of particulate media from two-dimensional images. *Journal of Colloid and Interphase Science* 248 (2), 419–428.

Terada, K., Miura, T., Kikuchi, N., 1997. Digital image-based modeling applied to the homogenization analysis of composite materials. *Computational Mechanics* 20 (4), 331–346.

Tomková, B., Šejnoha, M., Zeman, J., in preparation. Homogenization of plain weave composites with imperfect microstructure: Part ii—analysis of real-world materials.

Torquato, S., 2002. *Random heterogeneous materials: microstructure and macroscopic properties*. Springer-Verlag.

Torquato, S., Stell, G., 1982. Microstructure of two-phase random media. I. The  $n$ -point probability functions. *Journal of Chemical Physics* 77 (4), 2071–2077.

Wentorf, R., Collar, R., Shephard, M.S., Fish, J., 1999. Automated modeling for complex woven mesostructures. *Computer Methods in Applied Mechanics and Engineering* 172 (1–4), 273–291.

Whitcomb, J., Siregan, K., 1996. Effect of various approximations on predicted progressive failure in plain weave composites. *Composite Structures* 34 (1), 13–20.

Woo, K., Whitcomb, J.D., 1997. Effects of fiber tow misalignment on the engineering properties of plain weave textile composites. *Composite Structures* 37 (3–4), 281–417.

Woo, K., Whitcomb, J.D., 2000. A post-processor approach for stress analysis of woven textile composites. *Composites Science and Technology* 60 (5), 693–704.

Yeong, C.L.Y., Torquato, S., 1998a. Reconstructing random media. *Physical Review E* 57 (1), 495–506.

Yeong, C.L.Y., Torquato, S., 1998b. Reconstructing random media. II. Three-dimensional media from two-dimensional cuts. *Physical Review E* 58 (1), 224–233.

Yurgartis, S., Morey, K., Jortner, J., 1993. Measurement of yarn shape and nesting in plain-weave composites. *Composites Science and Technology* 46 (1), 39–50.

Yushanov, S.P., Bogdanovich, A.E., 1998. Stochastic theory of composite materials with random waviness of the reinforcements. *International Journal of Solids and Structures* 35 (22), 2901–2930.

Yushanov, S.P., Bogdanovich, A.E., 2000. Fiber waviness in textile composites and its stochastic modeling. *Mechanics of Composite Materials* 36 (4), 297–318.

Zeman, J., 2003. Analysis of composite materials with microstructure imperfections. Ph.D. Thesis, Klokner Institute, Czech Technical University in Prague.

Zeman, J., Šejnoha, M., 2001. Numerical evaluation of effective properties of graphite fiber tow impregnated by polymer matrix. *Journal of the Mechanics and Physics of Solids* 49 (1), 69–90.

Zeman, J., Šejnoha, M., 2002. On determination of periodic unit cell for plain weave fabric composites. *Engineering Mechanics* 1–2 (9), 65–74.

Zhang, Y., Harding, J., 1990. A numerical micromechanics analysis of the mechanical properties of a plain weave composite. *Computers & Structures* 36 (5), 839–844.